Ecological Indicators 126 (2021) 107683

Contents lists available at ScienceDirect

Ecological Indicators

journal homepage: www.elsevier.com/locate/ecolind

Changes in ecosystem services in a montane landscape impacted by major earthquakes: A case study in Wenchuan earthquake-affected area, China

Yanan Duan [a], Baofeng Di [a,b,*], Susan L. Ustin [c], Chong Xu [d], Qiang Xie [e], Shaolin Wu [a], Jierui Li [b], Ruixing Zhang [a]

[a] College of Architecture and Environment, Sichuan University, Chengdu 610065, Sichuan, China
[b] Institute for Disaster Management and Reconstruction, Sichuan University-The Hong Kong Polytechnic University, Chengdu 610207, Sichuan, China
[c] John Muir Institute of the Environment, University of California Davis, CA 95616, USA
[d] National Institute of Natural Hazards, Ministry of Emergency Management of China, Beijing 100085, China
[e] Sichuan Academy of Environmental Sciences, Chengdu 610041, China

ARTICLE INFO

Keywords:
Ecosystem services
Driving forces
Climate
Earthquake
Human activities

ABSTRACT

Earthquakes are one of the most serious natural disasters, threatening ecological balance and security. Ecosystem services (ESs) reflect the multiple functions of an ecosystem. However, based on catastrophic disasters, the contributions of various factors to ESs recovery have not been previously quantified. We follow recovery after the 2008 Wenchuan earthquake to gain insight into these processes. To quantify ESs, biophysical models were applied, including scenario simulation and Geodetector methods that were used to explore the driving forces. We concluded as follows: in overall study area, ESs showed an insignificant but undulating increase from 2001 to 2017, indicating the earthquake had slight but long-term effects. In the vegetated areas denuded by co-seismic landslides, the loss in ESs was twice that in non-denuded areas, and the damaged ESs did not recover to pre-earthquake levels by 2017. Overall, climate change was the main driving force, and the factors directly related to local climate had a more obvious impact on ESs especially elevation and geomorphic types. More than three quarters of study area showed ESs increases, with climate (accounting for 40.26%) and its multiple interactions with non-climate factors (accounting for 45.91%) contributed the most to ESs restoration, respectively at low elevations and in the subalpine mountains. Nearly a quarter of the study area was still degraded, of which the proportion of the area representing non-climate-driven factors had increased (accounting for 20.68%). The intensity of ESs degradation mainly concentrated in XI and X regions where co-seismic landslides were dense, which was one of the most influential non-climate factors. We therefore recommend that in the post-disaster reconstruction stage, more attention should be paid to restoration and maintenance of ecological service functions in areas with frequent secondary disasters, so as to maximize the benefits of post-disaster reconstruction projects and seek socio-economic and ecological environment collaborative development.

1. Introduction

Ecosystem services (ESs) refer to the various benefits that natural ecosystems provide to humans, including a range of provisioning, regulating, supporting, and cultural services (Mace et al., 2005). ESs closely link natural ecosystems and human society, ESs have economic significance, but also characterize the status and health of ecosystems (Peng et al., 2015; Sannigrahi et al., 2020), and play important roles in regional ecological balance, ecological homeland security, and global climate change. According to the Millennium Ecosystem Assessment (MEA, 2005), approximately 60% of ESs worldwide are in a degraded or unsustainable state. Ecosystems face enormous risks and challenges from natural hazards and anthropogenic stressors, which have exacerbated their eco-environmental vulnerabilities due to climate changes (Nguyen and Liou, 2019). Therefore, we ask under what conditions can the resilience of an ecosystem support its own recovery, especially within an ecosystem affected and damaged by multiple disasters.

Destructive earthquakes occur frequently around the world. The

* Corresponding author at: Institute for Disaster Management and Reconstruction, Sichuan University-The Hong Kong Polytechnic University, Chengdu 610207, Sichuan, China.
E-mail addresses: dibaofeng@scu.edu.cn (B. Di), slustin@ucdavis.edu (S.L. Ustin).

https://doi.org/10.1016/j.ecolind.2021.107683
Received 3 September 2020; Received in revised form 10 January 2021; Accepted 30 March 2021
Available online 12 April 2021

mountainous area of western China is both natural resources-rich and earthquake-prone, its fragile ecosystems (Liu et al., 2015; Zhen et al., 2019) are impacted by earthquakes and secondary disasters (e.g., landslides, debris flows, and floods) that kill and reduce vegetation cover on steep hillslopes, causing soil erosion, and enhanced overland flows (Ding et al., 2020; Wu et al., 2008). Earthquake and secondary disasters can cause a series of problems, directly and indirectly, affecting people living in these regions, such as loss of life and injuries, loss of shelter, and destruction of vital infrastructure (e.g., hospitals, schools, businesses), landscape fragmentation, loss of crops and food resources, deteriorating water quality and water availability, soil erosion that leads to future reduction of agricultural production, loss or deterioration of natural habitat and threatened or reduced biodiversity (Cui et al., 2011; Zhang et al., 2011). Each of these consequences of severe disasters lead to the degradation of ecological service functions, creating a vicious cycle. The impact of such damages might last for a long time, e.g., replacing a road or a railroad line, and repairing a hospital and replacing destroyed equipment, and rebuilding a home or business. Thus, regardless of whether the state of the damaged ecosystem spontaneously initiates recovery or continues to deteriorate long after an earthquake and its aftershocks happen, understanding the patterns of recovery or inability to recover, which still needs to be explored and understood.

The catastrophic "5.12" Wenchuan earthquake triggered thousands of landslides (Yang et al., 2018), and caused extensive damage over a wide 500,000 km^2 region along the foothills of the Himalayan Mountains throughout Sichuan Gansu, Shaanxi, and Yunnan Provinces (Di et al., 2010). In respect to vegetation, 1249.50 km^2 of vegetation on steep slopes was destroyed in this mountainous region, decreasing forests and other vegetation cover by 4.76% (Cui et al., 2012). In addition, 65.80 km^2 of bare soil was exposed as a result of the earthquake (Di et al., 2010), and additional erosion problems followed. The region impacted by the earthquake is a hotspot of biodiversity and the government has established more than 50 national forest parks and nature reserves (Bao, 2008), including Wolong Nature Reserve, Jiuzhai Valley National Park, and Sichuan Giant Panda Sanctuaries in this area. The main goal of this preservation was to protect biodiversity and natural ecosystems. Regions of severe calamity in Sichuan were managed like a sanctuary, protecting many rare and endangered animals and plants, such as egrets, golden monkeys, and 70% of the home range of iconic giant pandas in China. According to statistics, there were at least 263 important species (excluding insects), of which more than 60 species were among the first- and second-classes of national protected animals and plants (Bao, 2008). Of critical concern was that 655.84 km^2 of giant panda habitat (approximately 6% of its habitat) was destroyed (Ouyang et al., 2008). Threats from human activities, e.g. reclaiming new land to replace damaged farmland, illegal poaching and overgrazing to generate much needed income, have magnified since the earthquake (Zhang et al., 2014; Di et al., 2013). Under the dual stress of disasters and human activities, local biodiversity conservation has been recognized as a critical issue. Now, that more than 10 years has passed since the earthquake, we want to evaluate whether the ongoing impacts of the earthquake have been eliminated and whether the degree of recovery is consistent in comparison between geo-hazardous areas and non-geo-hazardous areas. In addition, the Wenchuan earthquake-affected area is an important ecological barrier in the upper reaches of the Yangtze River (Chen, 2008). However, its complex geological structure and hydrothermal conditions (from alpine valley to lowland plain, from seasonal rainstorm center to arid valleys) lead to large significant changes over short distances in ecosystem type and vegetation cover. Coupled with frequent engineering construction disturbance, its ecosystems are extremely fragile (Liu et al., 2015; Ouyang et al., 2008) and are thought to have a low capacity for resilience from major destructive events, such as severe soil erosion and increasing earthquake frequency that exacerbates the risk of ecological degradation (Bao and Pang, 2008). Once is the landscape has severely deteriorated, recovery becomes difficult if not impossible and the area becomes a degraded ecosystem.

Most studies focused on the spatiotemporal variation of NDVI to reflect the impact of the earthquake on ecosystems (Zhang et al., 2018a), and current research shows that surficial vegetation can recover to pre-earthquake level within 8 to 9 years after the earthquake (Gan et al., 2019), although some studies claim that an earthquake's impact might take two decades to disappear (Yunus et al., 2020; Yang et al., 2018). However, a generalized indicator like NDVI is not likely to fully reflect the ecosystem and its functionality (Chiang et al., 2014; Enming et al., 2016; Lin et al., 2006; Wang et al., 2012); comprehensive quantitative indicators and methods are still lacking to resolve recovery patterns.

Various ESs can quantify the status of different ecological functions. Thus, spatiotemporal changes of ESs may more comprehensively reflect changes that identify degraded ecosystems. Examination of how ESs change at specific pre- and post-earthquake times may help understand the extent of the damage, when vegetated sites are changed into bare land, and soil erosion becomes stronger and more severe. A short-term comparison of this may be insufficient to understand the trajectory of ecosystem recovery. ESs valuations have been typically based on monetary value and/or biophysical values (Campbell et al., 2020). Quantitatively comparing the pre- and post-earthquake monetary values of ESs over short periods following earthquakes have been documented. Previous studies suggested that the value of ESs that were destroyed by the Wenchuan earthquake was approximately \$520.04 $\times$ 10^6 (Chen et al., 2012), with loss of soil conservation services being most severe, followed by the carbon storage service and water-related ESs (Wang et al., 2012). Instead we calculated biophysical values of ESs to better compensate for the difficulties and disadvantages of evaluating intangible property by assigning a currency value and as a way to reflect the status of the ecosystem more objectively by ESs.

In addition, several factors have been thought to directly or indirectly contribute to the destabilization of ESs (Komugabe-Dixson et al., 2019; Sannigrahi et al., 2020), including natural conditions (e.g., changing climatic conditions, landform, vegetation cover) (Baniya et al., 2019; Liu et al., 2019; Zhang et al., 2020a) and human activities (e.g., land-use change, afforestation, urbanization) (Lee et al., 2020; Pham et al., 2019; Talukdar et al., 2020; Zhang et al., 2020a, 2020b). Given the frequent occurrence of earthquakes in the study area, earthquakes are considered to be an accidental factor outside the ecosystem itself that could similarly affect ESs like human activities. Clarifying these factors' relative contributions to the degradation and restoration of ESs will help understand and explain the mechanisms of change in ESs. And it further provides the government with scientific guidance on management of post-disaster recovery and reconstruction, ecological protection, and habitat management of rare and endangered animals and plants.

Because there has been less investigation about dynamic and long-term changes of quantitative ESs and analysis of the driving forces in an ecosystem disturbed by earthquakes, this study makes an effort to measure the biophysical values of ESs and to distinguish their dominant driving forces. Therefore, the primary purposes of this study were to: (1) quantitatively measure ESs in the Wenchuan earthquake-affected area from 2001 to 2017; (2) explore Spatiotemporal variation of ESs; (3) explore the driving forces of ESs changes.

2. Materials and methods

2.1. Study area

Wenchuan earthquake-affected area is located in the border of Gansu, Shaanxi, and Sichuan provinces, China, covering an area of 1.24 $\times$ 10^5 km^2 (Fig. 1). Topographically, it lies in a transitional zone between the lowest elevations and the higher mountains, with elevations from about 450 m to 5000 m. The area comprises canyons, mountains, plains, and hills. Climatically, it is at an intersection of the subtropical humid monsoon climate and the temperate continental semi-arid monsoon climate. The geological structure is complex, with the Longmenshan fault zone cutting across the center of a NE–SW transect.

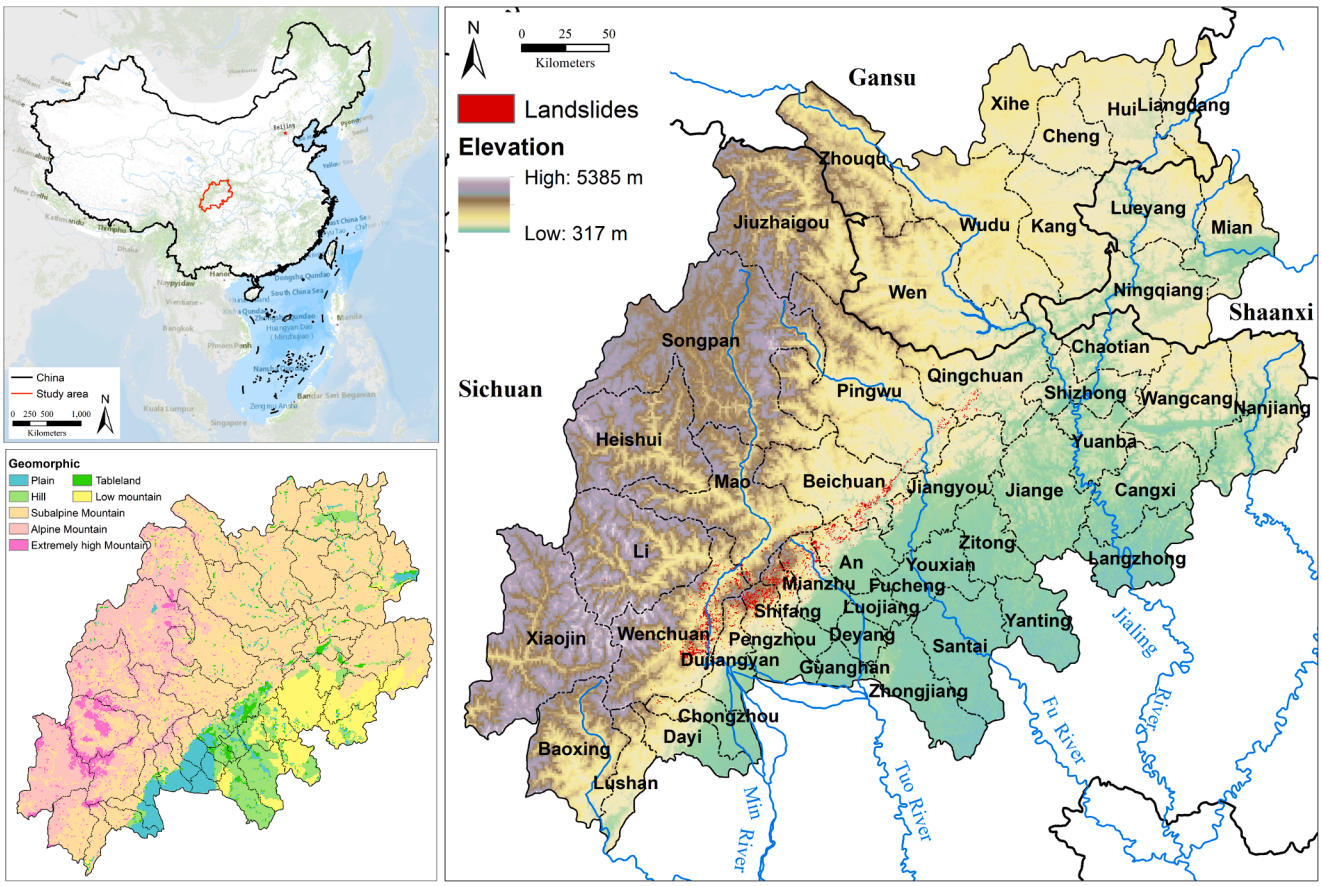

Fig. 1. Upper left panel: location of earthquake area within China, Lower left panel: geomorphic map of the earthquake area and Right panel: topographic map of the earthquake area and locations of landslides (shown in red) in the region of damage from the Wenchuan earthquake. (For interpretation of the references to colour in this figure legend, the reader is referred to the web version of this article.)

Table 1
Input datasets.

Dataset	Acronyms	Derived variables	Original spatial resolution	Original temporal resolution	Reference URL
MODIS MCD12Q1	VEG	Land Cover Type	500 m	yearly	https://search.earthdata.nasa.gov/search
MODIS MOD16A2	ET PET	Total Evapotranspiration Potential evapotranspiration	500 m	8-day	https://search.earthdata.nasa.gov/search
MODIS MOD13A3	NDVI	Normalized Difference Vegetation Index	1000 m	monthly	https://search.earthdata.nasa.gov/search
Meteorological data	TEM PRETSR	Temperature Precipitation Total solar radiation (calculated)	stations	daily	http://data.cma.cn/
Harmonized World Soil Database (HWSD)	SOT SOP	Soil types Soil properties	1000 m	invariant	https://westdc.westgis.ac.cn/data/611f7d50-b419-4d14-b4dd-4a944b141175
SRTM	ELE	Elevation	90 m	invariant	http://www.gscloud.cn
SRTM	SLO	Slope	90 m	invariant	http://www.gscloud.cn
GdpGrid_China	GDP	Gross Domestic Product	1000 m	5-year	http://www.resdc.cn/DOI (2017. DOI: https://doi.org//10.12078/2017121102)
PopulationGrid_China	POP	Population	1000 m	5-year	http://www.resdc.cn/DOI (2017. DOI: https://doi.org//10.12078/2017121101)
Landform type data of China	GMO	Geomorphic types	1000 m	invariant	http://www.resdc.cn/data.aspx?DATAID=124
Climate division of China	CLM	Climate types	vector data	invariant	http://www.resdc.cn/data.aspx?DATAID=243
Terrestrial ecosystem type data of China	ESY	Ecosystem types	vector data	invariant	http://www.resdc.cn/data.aspx?DATAID=105
Landslide density	LSD	Landslide density (spatial analysis)	1000 m	5-year	Chong Xu, et al (Xu et al., 2014, 2016)
Seismic intensity	SI	Seismic intensity	image	2008	http://www.gov.cn/govweb/wszb/zhibo262/content_1085953.htm

Because of its structural and climatic complexity, it is an important ecological transition zone with 24 species of plants and animals in the highest protected (first-class) status (Wang et al., 2012).

Additionally, secondary disasters have caused destruction of land and changes in ecological structure, increasing the impacts on ESs in the geo-hazardous area. Rock avalanches and landslides cause 98.73% of all types of geo-hazards in the earthquake region (Cui et al., 2012). Landslides were one of the most typical and common secondary disaster types. Thus, it is used as a criterion for dividing the overall study area (OSA) into the denuded area (DA) where vegetation has been lost from the surface and non-denuded area (NDA) to better understand the restoration of ESs under different degrees of damage. The DA was composed of 2521 landslides that were selected from the literature and used to represent the co-seismic landslide area that is larger than 50,000 m^2 (Xu et al., 2014, 2016). This remarkable area suffered secondary disasters and covered 0.50% area of the OSA. In summary, this paper defined three areas: OSA, NDA, and DA which were limited to changes only in areas that contained landslides.

2.2. Data and method

The dataset and main process used in this study were shown in Table 1 and Fig. 2. This process involves the following steps: first, ESs valuation; second, driving force analysis.

2.2.1. Value accounting of ESs

In the first step, biophysical values of ESs were calculated based on the *NPP* model, Miami model, and other collected datasets. The valuation method assumed that ESs were directly related to biomass, with *NPP* as a common variable increasingly used to represent biomass, and ESs were also related to other biophysical factors (such as slope, temperature, precipitation, etc.) (Carreño et al., 2012; Chen et al., 2019). Based on these methods, the values of ESs were calculated for each year from 2001 to 2017.

At the ESs valuation stage, remote sensing data were obtained from the ACCESS NASA EARTH SCIENCE DATA (https://search.earthdata.nasa.gov/search) for 2001 to 2017, that included land cover type (MCD12Q1) with a temporal scale of one year, NDVI (MOD13A3) with a temporal scale of one month, evapotranspiration (MOD16A2) with a temporal scale of eight days. Then data were mosaicked and reprojected. See Table 1 for details. Meteorological data were downloaded from the China meteorological science data-sharing service system (http://data.cma.cn/). The data included the daily average temperature, daily total precipitation, and daily sunshine period recorded by 40 meteorological stations in Wenchuan earthquake-affected area and nearby areas from 2001 to 2017, and the total solar radiation (TSR) was calculated from the sunshine period. Meteorological data were then interpolated at the same scale as the remote sensing data using Kriging. All data were resampled to 500 m to calculate Net Primary Productivity (*NPP*, g $C{\cdot}m^{-2}{\cdot}yr^{-1}$). Subsequently, adding the restrictive effects of several factors such as elevation, slope, temperature, etc., the value of ESs were calculated by the equations shown below (Barral and Oscar, 2012; Carreño et al., 2012; Chen et al., 2019; Ministry of Environmental Protection, 2015).

$$ES_t = \sum_{i=1}^{n} ES_i \tag{1}$$

where ES_t refers to the total value of various ESs, i is the ESs type, ES_i is the value of ESs for type i.

In this paper, four key ESs were selected, respectively: carbon storage, soil conservation, water provision, and biodiversity conservation. The equations for calculating the value of different ESs are as follows:

$$ES_{carbon} = NPP \times (1 - VC_{NPP}) \tag{2}$$

where ES_{carbon} is the value of carbon storage service. *NPP* is net primary productivity (g $C{\cdot}m^{-2}{\cdot}yr^{-1}$), VC_{NPP} is the coefficient of variation of *NPP* during the growing season.

$$ES_{soil} = NPP \times (1 - K) \times (1 - F_{SLO}) \tag{3}$$

where ES_{soil} is the value of soil conservation service. K is soil erodibility, F_{SLO} is a normalized slope.

$$ES_{water} = NPP \times F_{SIC} \times F_{PRE} \times (1 - F_{SLO}) \tag{4}$$

where ES_{water} is the value of water provision service. F_{SIC} is soil seepage capacity, F_{PRE} is normalized annual precipitation.

$$ES_{biod} = NPP \times F_{PRE} \times F_{TEM} \times (1 - F_{ELE}) \tag{5}$$

where ES_{biod} is the value of biodiversity conservation service. F_{TEM} and F_{PRE} are correction factors of annual temperature and precipitation respectively, F_{ELE} is normalized elevation.

As described in Fig. 2, three types of ES_t were defined based on various *NPP*: potential ES_t, actual ES_t, and disturbed ES_t. Potential ES_t is the hypothetical situation when ES_t was affected only by climate, as calculated by the potential *NPP* (obtained from the Miami model (Zhang et al., 2018b)). Actual ES_t is the situation where ES_t was affected by all possible factors (climate change, human activities, afforestation,

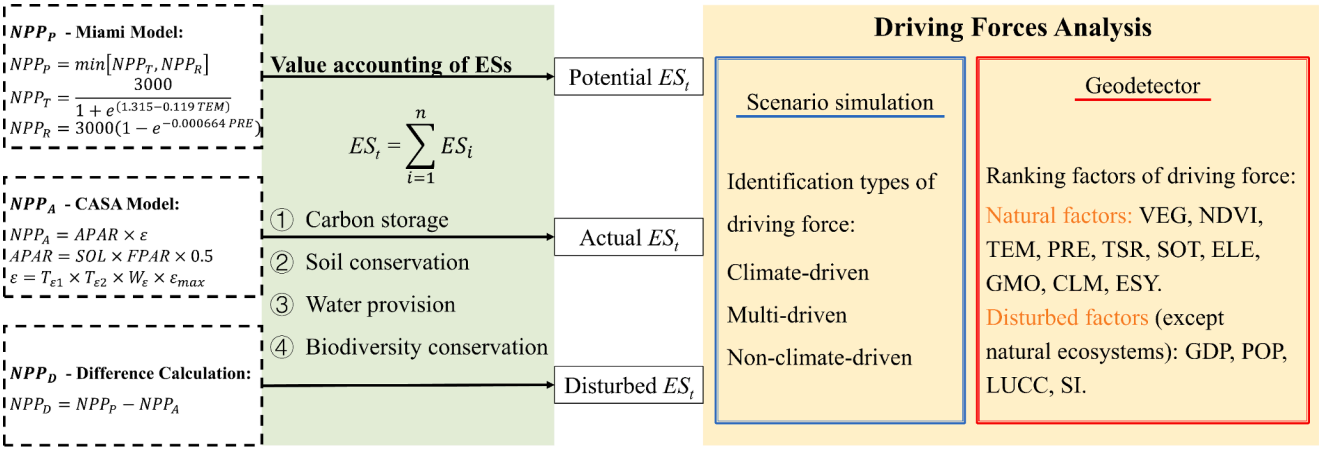

Fig. 2. Flow diagram (Acronyms in Table 1. *NPP*, coefficient of variation of *NPP*, soil erodibility, slope, soil seepage capacity, precipitation, and temperature are related to four types of ESs. In the calculation of potential ES_t, actual ES_t and disturbed ES_t, *NPP* respectively stands for NPP_P (NPP_P is potential *NPP*), NPP_A (NPP_A is actual *NPP*), and NPP_D (NPP_D is a value influenced by factors outside the natural system). For the explanation of other parameters and calculation formulas, please refer to the literature (Gao et al., 2016; Zhang et al., 2018b)).

earthquakes, and secondary disasters), as calculated by the actual *NPP* (obtained from the CASA model (Zhang et al., 2018b)). Disturbed ES_t is the non-climate-induced change when ES_t was affected by other factors except climate (factors considered in this paper are human activities, afforestation, earthquakes, and secondary disasters), as the difference between potential ES_t and actual ES_t. If the value of disturbed ES_t was less than 0, indicating that non-climate factors had a positive effect on helping the actual ES_t increase, and as the value decreases, the stronger the impact. If the value of disturbed ES_t was greater than 0, the effect of the non-climate interference was to reduce the actual ES_t, and as the value of ES_t increases, the stronger the impact.

2.2.2. Driving forces analysis

In the second step, two methods were used to explore the driving forces of ES_t, a scenario simulation method and Geodetector method.

The scenario simulation method of an *NPP* driving force (Wang et al., 2016) was introduced into ESs research (Wang et al., 2020). Linear regression analysis was used to detect long-term trend changes in each pixel, and the slope rate (θ) was calculated following Eq. (6) (Zhang et al., 2018b).

$$\theta_X = (n \times \sum_{j=1}^{n}(j \times X_j) - \sum_{j=1}^{n} j \sum_{j=1}^{n} F_j)/(n \times \sum_{j=1}^{n} j^2 - \left(\sum_{j=1}^{n} j\right)^2) \quad (6)$$

where n is consecutive years; j is the numerical order of the year from 2001 to 2017, and X_j is the value of factor X in year j. A positive θ value suggests a linear increasing trend (i.e., factor X increases during the study period) and vice versa (i.e., factor X decreases).

Consequently, based on the three types of ES_t above, six scenarios were constructed based on their θ, which reflects the types of dominant driving forces of ES_t and their changing trends (see Table 2).

Geodetector method can effectively identify the relationships between multiple factors and geographical phenomena and has been used to detect spatial heterogeneity and identify driving factors (Wang and Xu, 2017). The Geodetector software was easily accessible from the website (http://www.geodetector.cn/). In order to explore the driving force of ESs changes covering nearly 20 years, the factor detector module in Geodetector tended to be used for detecting the relative importance of factors, and the interaction detector module was applied to evaluate the accountability of the combined effects on the ESs (Peng et al., 2019). The vast majority of environmental and social factors were considered as the relevant factors, and these are divided into natural factors, and other factors (e.g., man-made or disaster). Natural factors include TEM, PRE, TSR, SOT, ELE, GMO, CLM, and ESY. Man-made and disaster factor group includes GDP, POP, LSD, and SI (see Table 1).

During the study period, the elevation, geomorphic types, soil types, climate types, and seismic intensity of the Wenchuan earthquake remained relatively stable in the study area, so invariant data were used. Similarly, changes in types of land use and terrestrial ecosystems were relatively small and fragmented, so a middle year (2010) of these datasets was chosen to represent the entire study period (Zhao et al., 2017). The remaining datasets were quite different over the 17 years, so their θ represented past trends. These data form the explanatory variables dataset for Geodetector. Furthermore, the explained variable data was the θ of ESs, also obtained by this equation.

According to the input requirements of Geodetector, the explanatory variables required discrete data. Therefore, after several experiments in ArcGIS 10.7, a better classification method was selected to reclassify explanatory variables into 6–8 classes.

Table 2
The six possible scenarios of the relative role of climate and other factors on ES_t changes.

	θ of actual ES_t	θ of potential ES_t	θ of disturbed ES_t	Description
Scenario1	+	−	−	Other factors (100%) contribute to the actual ES_t increase.
Scenario2	+	+	−	Both climate change and other factors contribute to the actual ES_t increase.
Scenario3	+	+	+	Climate change (100%) contributes to the actual ES_t increase.
Scenario4	−	+	+	Other factors (100%) contribute to the actual ES_t decrease.
Scenario5	−	−	+	Both climate change and other factors contribute to the actual ES_t decrease.
Scenario6	−	−	−	Climate change (100%) contributes to the actual ES_t decrease.

3. Result

3.1. Temporal characteristics of ESs

Fig. 3A shows actual ES_t in OSA has an undulating upward trend that does not reach a significant level, but with an increase of approximately 8.89 g C·m^{-2}·yr^{-1}. After the earthquake, actual ES_t declined slightly between 2008 and 2010, decreasing by about 152.59 g C·m^{-2}·yr^{-1}. Then, actual ES_t grew at a relatively rapid rate and exceeded the 2008 level in 2013. It seems that actual ES_t has recovered to the pre-earthquake level. Combining Fig. 3B, the curve of actual ES_t in the NDA is almost the same as in OSA, showing similar rules. This was because despite the great earthquake magnitude and strong damage, the geologically destroyed area was relatively small and the entire study area was not as completely and severely damaged as originally believed. The curves of actual ES_t and potential ES_t are pairwise compared, and the changes of the two variables are highly consistent, which means that actual ES_t in OSA and NDA was mainly subject to climate change.

In order to avoid the extensive study area, masking only the characteristics of the area that experienced the greatest impact of the disaster, with complementary exploration in the DA was effective. Different time-varying characteristics are shown in Fig. 3C. The actual ES_t in the DA shows an insignificant but downward trend, decreasing by approximately 16.31 g C·m^{-2}·yr^{-1}, so, the situation of ESs in the DA is not optimistic. Furthermore, the potential ES_t has an increasing trend significantly from 2007 to 2008, the actual ES_t should have risen with the potential ES_t, but it declined in a downward trend at the same stage, which indicated that the actual ES_t was affected by non-climate factors this year and it caused a large loss in ecosystem service values.

Fig. 4 shows the actual ES_t for the DA and NDA damage levels, which shows evidence that the actual ES_t in the DA has not recovered to pre-earthquake levels. As seen in Fig. 4, the actual ES_t in the DA was higher than the actual ES_t in the NDA before 2008. The geologically damaged area was mainly dominated by forest ecosystems before the earthquake, this area had better conditions in its natural environment and provided more products and services for human beings than in non-geologically damaged areas. However, the actual ES_t in the DA was less than that in the NDA since 2008. At the same time, the pre-earthquake average value of the actual ES_t in the NDA increased by 38.71 g C·m^{-2}·yr^{-1} to the post-earthquake average value in the NDA. The opposite occurred in the DA where the pre-earthquake average value actual ES_t decreased by 270.07 g C·m^{-2}·yr^{-1} to the post-earthquake average. These signs mean that the actual ES_t in the DA is significantly different than the actual ES_t in the NDA. Based on the actual situation, the Wenchuan earthquake and secondary landslides could be considered the main causes of this difference.

From the perspective of the disturbed ES_t, the ES_t of OSA and NDA did not fluctuate sharply during the entire study period, but the

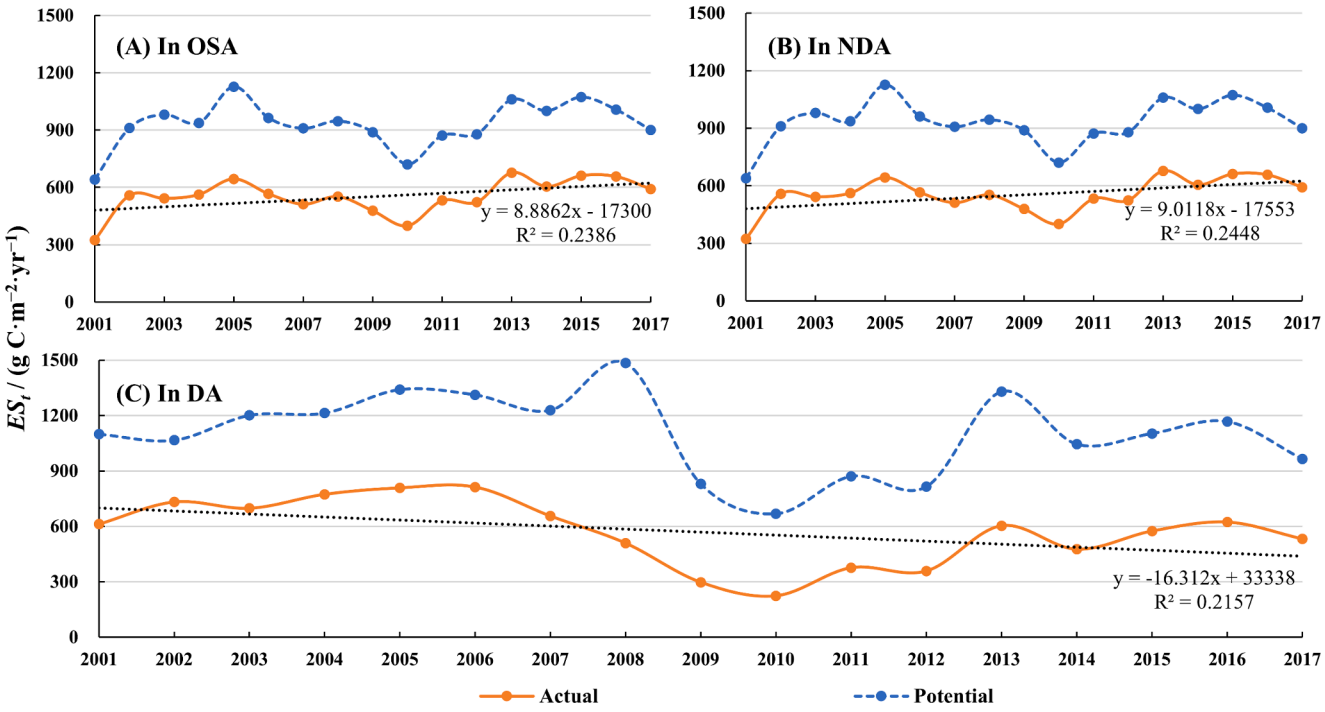

Fig. 3. Time series curves of potential ES_t and actual ES_t in different areas.

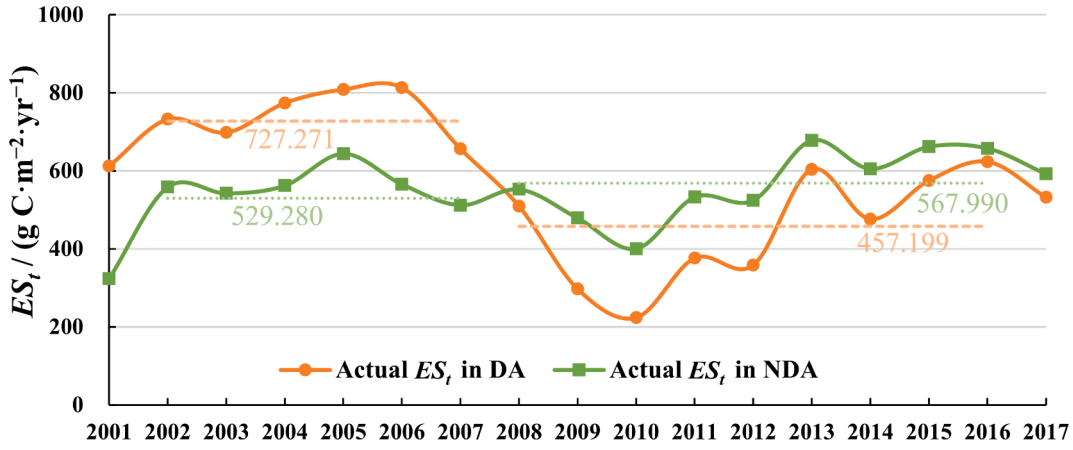

Fig. 4. Comparison of actual ES_t in the DA and NDA.

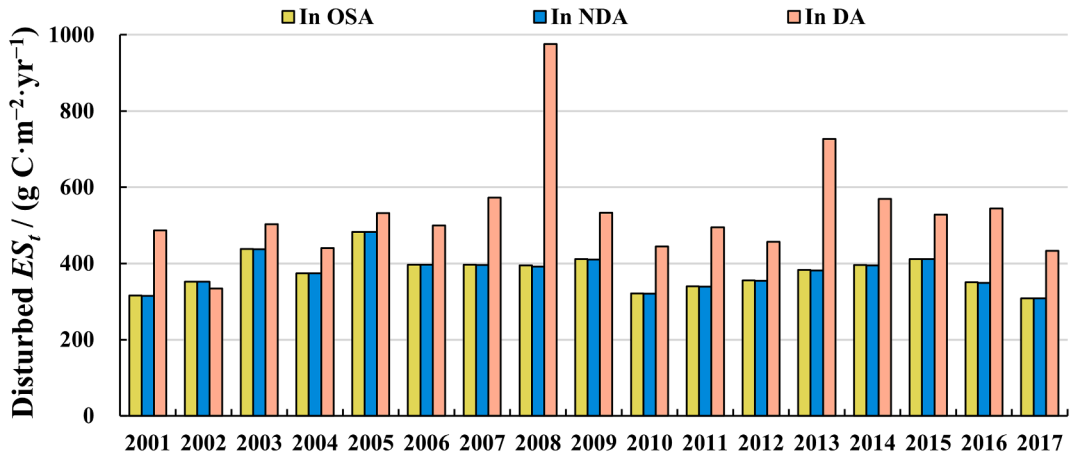

Fig. 5. Time series curves of disturbed ES_t.

disturbed ES_t in the DA declined following the earthquake (Fig. 5). Disturbed ES_t of DA reached a peak in 2008, which suggested the losses of ESs caused by non-climate factors were severe in this year, and it reached 976.00 g C·m^{-2}·yr^{-1}, more than double the disturbed ES_t in the NDA, and even reached 1.8 times the average value throughout the study period. The impact of geological damage on ESs was extremely obvious in the year of the earthquake, which was 494.67 g C·m^{-2}·yr^{-1} more than the pre-seismic average of DA and exceeded the pre-seismic average of 582.69 g C·m^{-2}·yr^{-1} for NDA.

3.2. Spatial characteristics of ESs

The detailed spatial variation of the multi-year average actual ES_t, potential ES_t, and disturbed ES_t are shown in Fig. 6. In Fig. 6A, the high-value areas of potential ES_t are mainly concentrated in the subalpine mountains of the central area and southern low-elevation areas (low elevation mountains, hills, tablelands, and plains). The spatial distribution of actual ES_t is similar to the distribution of potential ES_t, but with lower values for most of the area, interference factors were responsible for these differences. In Fig. 6B, actual ES_t is high in the subalpine mountains, and followed by the southern low-elevation areas, but low in western extremely high and alpine mountains (see Fig. 1 for reference). Moreover, disturbed ES_t is shown in Fig. 6C, which represents the impact of disasters and human activities on the ESs. The significantly disturbed areas are mainly distributed along the Longmenshan fault zone. High-value areas are also located at the border of Jiange, Shizhong, and Yuanba counties, especially in the north of Jiange County. ESs in the areas surrounding the rivers also suffered losses, such as the Deyang County section of the Tuo River, and the Fucheng-Santai County section of the Fu River.

Due to the outstanding growth of the disturbed ES_t in 2008, Fig. 7 shows the spatial characteristics of the ES_t during that year. Along the Longmenshan fault zone has the highest values in the whole study area, concentrated in the XI seismic intensity region near the epicenter. The results show that the areas where ES_t was most affected by non-climate interference in 2008 were concentrated in several counties of Jiange, Shizhong, Yuanba, Wenchuan, Pengzhou, Shifang, and Mianzhu.

3.3. Driving forces of ESs using scenario simulation

The results of the scenario simulation provide two important pieces of information, one is the trend of actual ES_t, and what is the type of driving force for actual ES_t change, climate or non-climate dominant, or multi-factor dominant.

From 2001 to 2017, about 75.53% area of OSA is in an upward trend, most of which are located in plains, hills, low elevation mountains, and in the northeastern part of subalpine mountains. The positive area is an important support for the gradual growth of actual ES_t in OSA, of which climate-driven and multi-driven factors accounted for 40.26% and 45.91% respectively, and contributed the most to ESs recovery (accounting for >85%). However, 24.42% of OSA is declining, mainly in the western alpine mountains and Longmenshan fault zone near the epicenter, for which non-climate-driven factors accounted for 20.68%, higher 6.85% than those in areas of increasing ESs.

Actual ES_t was mainly driven by climate for nearly 20 years, followed by the multi-driven dominance of a combination of climate and non-climate factors. These two driving forces account for more than 80% of the area of OSA. As shown in Fig. 8B, firstly, the climate-driven areas (43.16% area of OSA) are in the western alpine and highest mountain regions and southern low-elevation areas; the positively correlated trend accounts for 70.45% of the climate-driven area. Secondly, the multi-driven areas (41.34% area of OSA) are northwest of the subalpine mountains, and are positively correlated for 83.87% of the area.

Fig. 8C is a comprehensive diagram of Fig. 8A and Fig. 8B. As can be seen, the southern low-elevation areas show climate-dominant increases, which indicates that disturbance factors (especially human activities, as numerous residents and settlements, are gathered here) had a negative effect on ESs here, but this loss was offset because of climate-dominant increases in ESs. The climate positive effect was greater than the negative effect of man-made impacts, which makes actual ES_t ultimately increase during the study period. Moreover, the increasing actual ES_t by non-climate- dominant factors was 10.45%, which occurred mainly in several counties of Gansu Province, such as Wudu, Kang, Cheng. Regarding the distribution of actual decreasing ES_t areas, the areas where non-climate and multi-factors dominated the actual ES_t

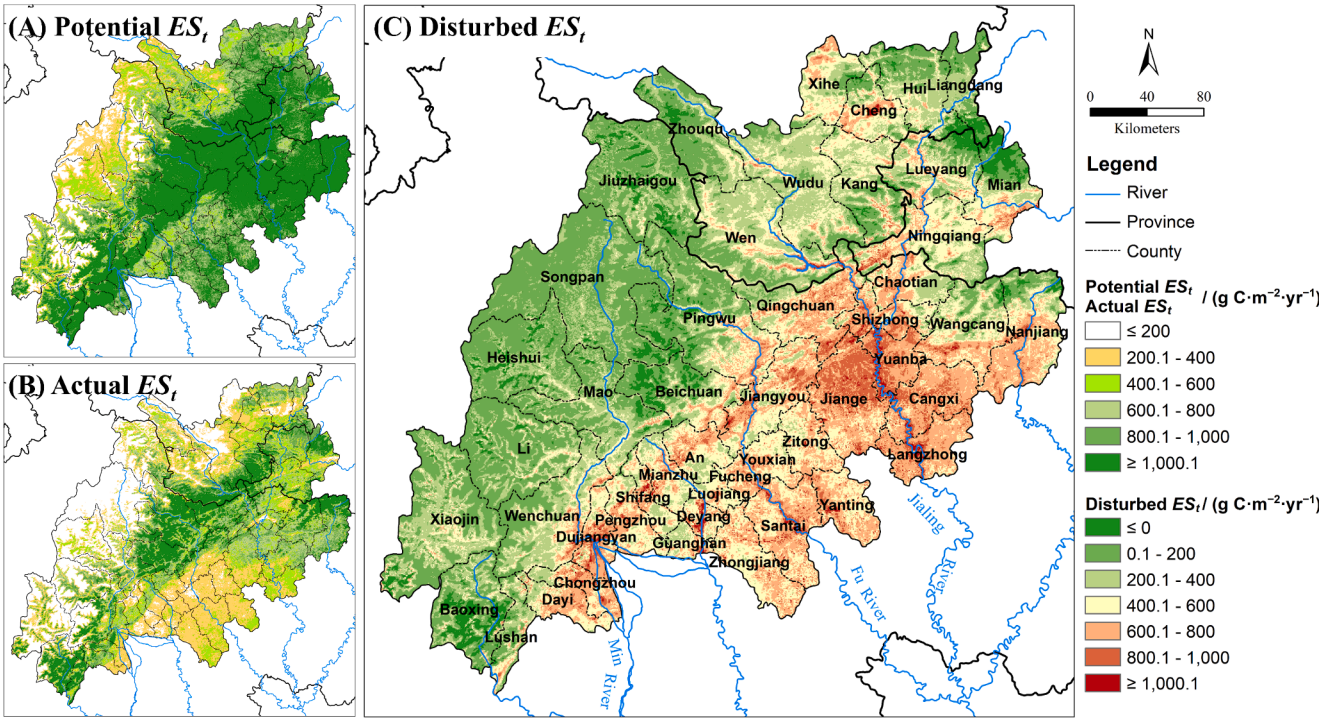

Fig. 6. Distribution of multi-year average ecosystem services.

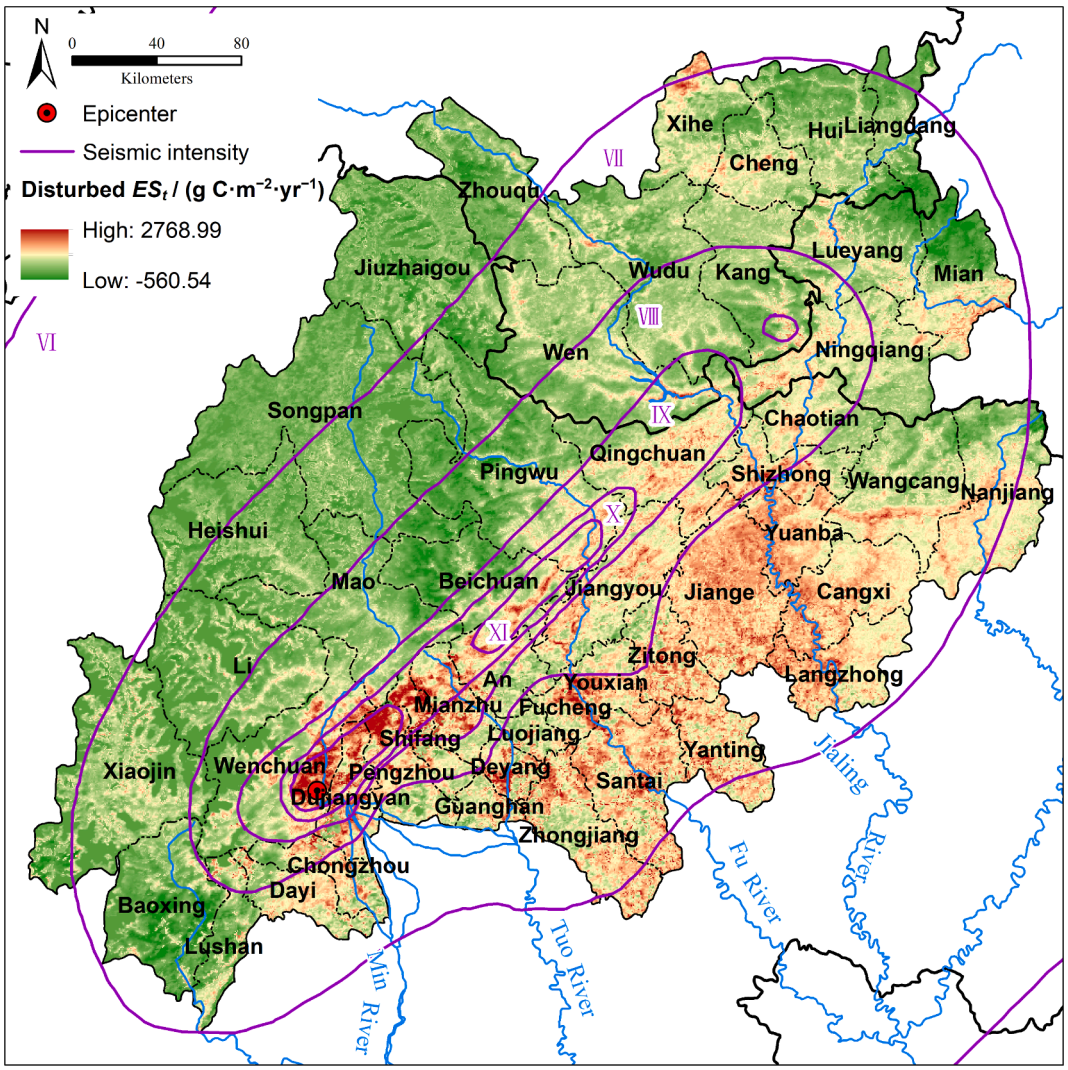

Fig. 7. Distribution of disturbed ES_t (2008).

decrease were more scattered, mostly concentrated in the XI and X seismic intensity regions that were the most severely damaged by co-seismic landslides. Co-seismic landslides were the main non-climate factor here. The non-climate-dominant ES_t decreasing areas were widely scattered in the west of OSA, the areas distributed on the plain were highly consistent with the cities and their surroundings, such as Dujiangyan, Deyang, Fucheng. It was reasonable to believe that the changes were closely related to human activities represented by urban expansion.

Focusing on the DA, 68.09% of the area is still in a declining state more than 10 years after the earthquake, and the non-climate-driven reduction is only 8.52% of the DA. Compared to the NDA. The proportion of the DA with a reduced state of ES_t is higher than that the NDA ES_t by about 43% (NDA actual ES_t is reduced by 24.20%). The proportion of non-climate-driven reduction in the DA is about 4% higher than in the NDA (5.03% of the NDA has decreased). The recovery state of ESs in the NDA is acceptable, but the ESs in the DA is still problematic. For residents who rely on the DA and its surroundings for production and resources, the benefits they received from the ecosystem have had lasting losses due to the earthquake. It is possible to enhance management actions and ecological compensation in the DA during the restoration and reconstruction process to change the trajectory of the decline and improve ESs conditions for the people who rely on them.

3.4. Driving forces of ESs using Geodetector

The Geodetector was used to uncover what environmental factors influence the level of ESs by calculating the q value (the explanatory power of factors on ESs), which represents the ability of the independent variable to explain the dependent variable. The higher the value, the stronger the explanatory power, which means that the independent variable factor, shows greater effect on the dependent variable. Geodetector results showed that natural factors (see Table 1 for datasets) were the most important type of driving force affecting ESs changes over the past nearly 20 years, and the explanatory power of the natural factor group was much stronger than that of the man-made and disaster factor groups with the sum of the former q value being 0.40, and the latter was only 0.18 (see Table 3). Elevation (ELE) was the primary driving factor, which is represented by its spatial pattern and it explained 15% of actual ES_t changes. This factor was followed by geomorphic types (GMO). ELE and GMO were closely related to the local climate through controlling atmospheric circulation, temperature, precipitation, etc., and they were the comprehensive and basic conditions for the formation of local climate, so their explanatory power was stronger. GDP and LSD were the main non-climate driving factors, reflecting that human activities and secondary disasters also had a greater effect on instability of ESs. From 2001 to 2017, the factors are ordered by magnitude of the q value: ELE > GMO > GDP > SOT > LSD > CLM > POP > SI > TSR > TEM > ESY > PRE.

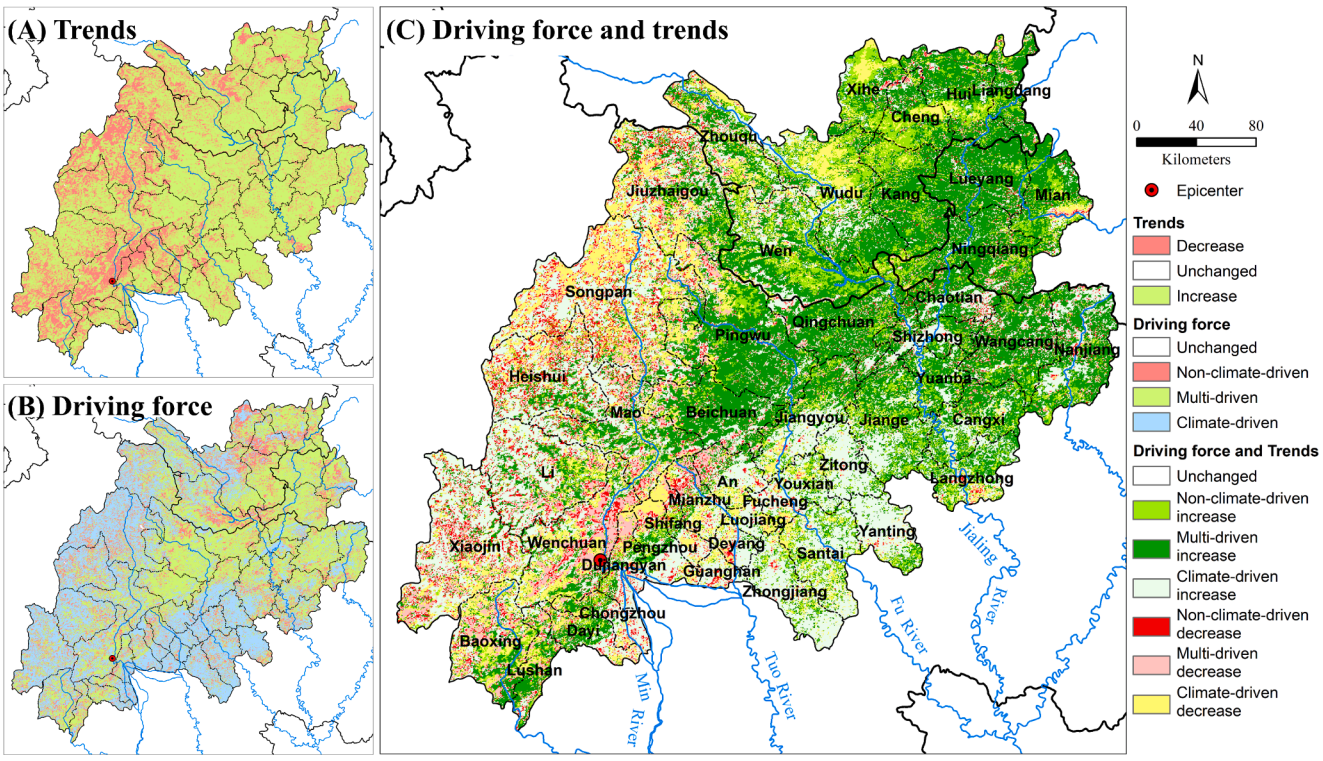

Fig. 8. Driving force distribution of actual ES_t.

Table 3
Factor detection results for individual factors.

variable	ELE	GMO	GDP	SOT	LSD	CLM	POP	SI	TSR	TEM	ESY	PRE
q value	0.15	0.09	0.06	0.06	0.05	0.04	0.04	0.03	0.02	0.02	0.01	0.01
p value	0.00	0.00	0.00	0.00	0.00	0.00	0.00	0.00	0.00	0.00	0.00	0.00

GDP was the first non-climate factor, representing the impact of human activities on ESs. However, its manifestation in the results of scenario simulation was not obvious. The high value of GDP was mainly distributed in the low elevations as plains and hills, where the physical conditions supported a wide range of human activities, meaning the higher potential ES_t and more ESs were created here. Thus, the negative effects of human activities on ESs were offset by substantial growth of climate-driven ESs, forming the observed heterogeneity.

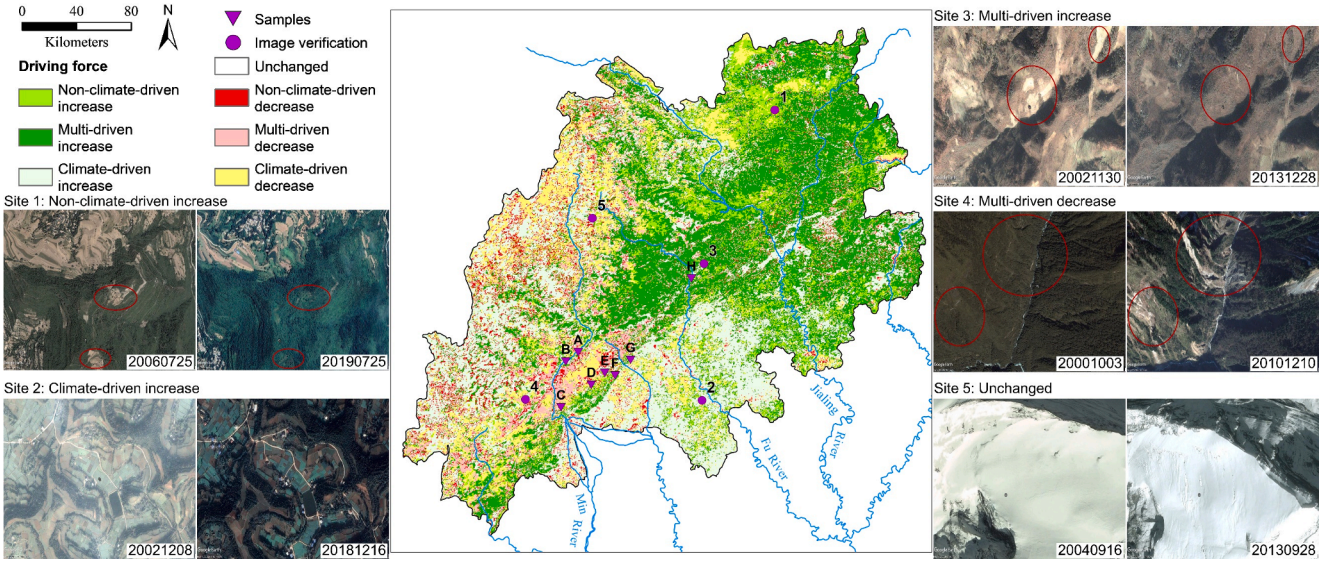

Fig. 9. Verify site distribution and image comparison.

3.5. Validation

3.5.1. Remote sensing image comparison

Several sites were selected to verify surface changes by remote sensing images. Most places are in mountainous areas, and high-resolution remote sensing images were limited. In order to exclude seasonal effects, the images selected were from the same month or the adjacent month as necessary. Under this rule, some later images were in 2018 and 2019, but these images basically reflected surface changes during the study period.

The spatial distribution and images of sites are shown in Fig. 9. Site 1 (upper left panel) is located in the subalpine mountains in the northeast of the study area. This is a typical area where the actual ES_t was driven by non-climate variables. At this site, there was less undulating terrain and fewer villages. Compared with its early and late images, most of the original bare land was covered by newly grown vegetation, some grasslands gradually became shrublands, and the overall trend was better. Site 2 was an actual ES_t-increased area driven by climate, located in the southern hills. It was surrounded by many villages and cultivated land. Because of fewer geo-hazards in the region, we can speculate that its ESs interference mainly comes from frequent human agricultural production activities. Its natural vegetation remained basically stable based on a comparison of the images. Therefore, favorable climate change for crops may be the reason for the continuous improvement of its ESs, such as rising temperatures, increased solar radiation, and more precipitation. Site 3 was a multi-variable driven increased area, where the actual ES_t was driven by the combined action of climate and non-climate. It is a moderately topographically rough mountainous area with few surrounding villages, affected by farming on low slopes. Comparing the two images, the vegetation cover had increased, and some slopes with poor vegetation growth had also increased in cover.

Degraded areas of ESs are shown in Fig. 9. Site 4 was in a multi-driven area that decreased ES_t, which was reduced by both climate and non-climate factors. This site is located on the edge of a river with complex terrain. From the images, it suffered severe geo-hazards; there was no bare ground before the Wenchuan earthquake, but large-scale landslides have occurred since then on the steep mountainsides along the river. Numerous post-earthquake landslides destroyed the original vegetation that provided local ESs and threatened the downstream ecosystems, resulting in a huge loss of the living environment, agricultural production, people's livelihoods, and the degradation of ESs. Very few areas changed only slightly during the last 20 years, mainly at Site 5, which is a high-elevation alpine site in the mountains. Due to all year snow covering and little human activity, it has remained almost unchanged.

3.5.2. Field sampling comparison

In addition to the visible vegetation changes in the images, we also monitored the soil nutrients for biogeochemical changes, to show the ecological state from different considerations after the earthquake. A total of 16 field samples in 2011 and 2018 were divided into eight groups (see Fig. 9 for locations). Each group contains a sample from land damaged by landslides after the earthquake (DS), and the other is a undamaged control sample (CS) in an adjacent area (to ensure the same geological and climatic conditions). We then calculated the change rate of soil nutrients (see Table 4), subtracted the value of 2011 from the value of 2018 and divided by the value of 2011.

Thus, the structure of the soil at the damaged sites has not been fully restored after being destroyed by the earthquake. The soil moisture of the DS was also less than that of the CS, and soil moisture in the DS decreased more, indicating that the water storage capacity of the soil at the damaged sites was weakened. The soil bulk density of the DS was greater than that of the CS, resulting in a hardening tendency. The soil of the CS was loose and suitable for cultivation. Thus, the material supply, one of the ecosystem services provided by the soil was also reduced in the damaged sites. The soil organic matter and nutrient elements of the DS were less than that of the CS. The recovery of organic matter, total N, available N, total P, and available K of the DS was less than that of the CS. Due to the earthquake destruction, the soil structure has not recovered after being destroyed in the landslides.

After image comparison and field sampling comparison, the experimental predictions were found to be basically consistent with the actual situation. From the results of scenario simulation and Geodetector, the driving force types and individual factors were mutually confirmed.

4. Discussion

The high values of ES_t along the Longmenshan fault zone may require further explanation. The Longmenshan fault zone of high-value disturbed ES_t, shown in Fig. 6C, is densely populated and experiences frequent earthquakes, and it could be expected that human activities and natural disasters threatened and disrupted the local ESs. Secondly, the area along the Tuo and Fu rivers continuously distributed many settlements and cultivated lands, which might be the reason for the high disturbed ES_t. Thirdly, the junction of Jiange, Shizhong, and Yuanba counties is at the location of Guangyuan City, where rapid urbanization has directly resulted in high disturbed ES_t.

The DA were the key areas of ESs regulation. These are areas that were directly damaged by the earthquake, causing thousands of landslides, and the impacts lasted for years to decades (Yang et al., 2018). Meanwhile, the increase of loose unstable materials after the

Table 4
Change rate of soil quality.

ID	Damaged or not	Soil moisture/ %	Soil bulk density/ %	Organic matter/ %	Total N/ %	Available N/ %	Total P/ %	Available P/ %	Total K/ %	Available K/ %
A	Yes	−0.74	0.80*	−0.96	−0.93	−0.95	−0.48	−0.80	−0.15	−0.70
	No	0.39	−0.34	6.51	4.54	10.13	0.29	/	−0.15	3.03
B	Yes	−0.53	0.48*	−0.74	−0.60	−0.69	−0.35	2.58*	−0.24	−0.02
	No	−0.02	−0.40	5.02	4.13	3.56	0.53	1.05	−0.08	1.76
C	Yes	−0.53	0.03*	7.47	4.58	1.00	0.14	14.20*	−0.05*	−0.09
	No	−0.01	−0.17	0.66	0.46	1.06	0.14	2.09	−0.25	−0.03
D	Yes	−0.61	0.54*	−0.47	−0.65	−0.70	−0.33	1.27	0.17*	−0.66
	No	−0.24	−0.08	0.09	−0.15	0.02	0.33	3.41	−0.19	0.99
E	Yes	−0.51	0.22*	0.40	−0.08	−0.41	−0.16	5.82*	0.11*	0.63
	No	−0.03	−0.09	0.19	0.21	0.04	−0.34	−0.09	−0.19	1.00
F	Yes	−0.30*	−0.32	0.02	0.77	1.26	0.10*	/	0.37	3.31*
	No	−0.57	0.24	0.22	−0.12	−0.46	−0.30	0.05	0.13	0.29
G	Yes	−0.08	−0.05*	−0.43	0.17	0.71	−0.50	/*	−0.45	0.18
	No	−0.17	−0.22	0.55	0.51	0.28	−0.03	7.75	0.05	0.49
H	Yes	−0.84	0.30*	1.49	0.18*	2.70*	0.05*	0.88*	0.07*	0.28
	No	−0.13	0.46	−0.84	−0.79	−0.86	−0.88	−0.94	−0.19	−0.71

Note: "/" indicates that the value of 2011 is missing and cannot be calculated, and "*" indicates that the measured value of the damaged site sample exceeds that of the control sample.

earthquake, coupled with the influence of seasonal rainfall, mountain topography, and human land use factors, created conditions in which new landslides were prone to occur, which themselves had an additive negative impact on the DA, resulting in typical destruction of vegetation cover, habitat fragmentation, soil erosion, soil degradation, and other ecological problems (Cui et al., 2012). DA require additional protection to maintain ESs and enhance recovery, for future earthquakes and other disasters.

Because DA and NDA sites showed opposite trends in potential ES_t and actual ES_t in 2008 as seen in Fig. 3C, it is reasonable to interpret that the decrease in ES_t that year was caused by earthquakes and co-seismic landslides. Following the consistent trends in potential ES_t and actual ES_t for both DA and NDA sites in the following two years, it is reasonable to interpret the decrease in ES_t was largely driven by climate affecting the larger region. After the local ecosystems were damaged in 2008, ES_t continued to decline due to climate impacts, but this turned into restoration in 2011. The DA is located in the Longmen Mountain in the giant panda habitat, where we recommend that management should focus on enhancing vegetation and biologic assets to produce a wide range of ecosystem services vital to supporting the panda habitat, and restoration strategies should be adjusted based on their different stages of disaster recovery to improve their ecological states. In a short time after the earthquake, the denuded sites were easily eroded without vegetation cover to protect the topsoil. Soil erosion, lost nutrients, and organic matter provided new material sources downslope for other mountain hazards. Therefore, ecological engineering methods should be introduced as quickly as possible to stabilize these unstable landslide sites and mitigate the possibility of debris flows and additional landslides. Some studies have pointed out that the continuous decrease in the co-seismic landslides area is often associated with accelerated rates of post-earthquake vegetation regeneration (Chen et al., 2020; Shafique, 2020). Consequently, a re-planting vegetation plan should be the primary strategy for post-disaster rejuvenation in this stage. The native pioneer plant species can be rapidly established in the denuded sites to form natural vegetated buffer strips that prevent erosion (Lin et al., 2006). A feasible management measure is to restore the key structure, composition, and functional characteristics of the native vegetation system, starting with native pioneer plant species, to reduce continued degradation of the ecosystem caused by further disturbance and enhance its resilience to the original damage. In the long-term recovery stage, with the help of nature's own robust ability to regenerate vegetation in landslides (Lin et al., 2006), additional human disturbance should be avoided or at least reduced, which could change the natural cycle of recovery and forest inheritance. Meanwhile, policy and ecological restoration projects are effective measures for ecosystem restoration (Lu et al., 2018; Zhou et al., 2020), management should strictly protect the landscape areas that have special and important ecological functions, and appropriately consider the trade-offs and synergy of ESs in order to maximize the comprehensive impact of ESs in construction and management.

The method used in this study has the potential to solve problems encountered by decision makers in planning local and regional scale post-disaster reconstruction and management. However, the valuation of ESs shown in this paper is mainly based on the assumption that a good natural foundation will provide better ESs, which represents its biophysical significance. The economic significance of the disaster and recovery was not evaluated here, but this needs to be carried out in future studies. In addition, this study was limited by data resolution and more precise data may increase spatiotemporal accuracy that will lead to more nuanced restoration methods in future studies. Several other factors that were not considered here due to lack of information may also lead to a better understanding of the degradation of ESs, thus expanding the range of factors will improve in future research.

5. Conclusion

This paper dynamically and quantitatively measured the value of ESs in Wenchuan earthquake-affected areas from 2001 to 2017 using a biophysical model to understand the long-term ecological status and evaluated the respective contributions of climate and human activities and the earthquake based on scenario simulation and Geodetector methods. The method of this paper introduced and combined *NPP* scenario simulation and Geodetector analysis in research on the driving force of ESs, which provides a new perspective of ideas and methods and can further quantify the contribution of each driving force factor. The combination of the two methods not only reaffirmed each other but provided deeper understand of the role of each factor in ESs.

During the study period, the biophysical values of ESs showed an insignificant increase across the topographically complex region, namely the earthquake affected the overall study area slightly. However, the ESs loss caused by the co-seismic landslides was twice that normal in the DA, and the damaged ESs in the DA have not yet recovered after 10 years to their pre-earthquake levels.

Climate change was the main driving force (43.16% area of OSA), followed by multiple environmental conditions driving a combination of climate and non-climate factors. In the areas where ESs are increasing, the two driving forces contributed to the recovery of more than 80% of the area. The climate-driven ESs were mainly at low-elevations, while the multiple drivers to ESs increases were mainly found in subalpine areas. The areas where ESs was reduced was mainly concentrated in the seismic intensity XI and X regions where co-seismic landslides were densely distributed, and the proportion of non-climate factors increased to 20.68%. Co-seismic landslides can be regarded as an important non-climate factor. The contributions of various factors affecting the ESs were ranked as follows: ELE > GMO > GDP > SOT > LSD > CLM > POP > SI > TSR > TEM > ESY > PRE (see Table 1). ELE and GMO, which are closely related to local climate, cannot be artificially modified over large-scales. Therefore, in the post-disaster reconstruction stage, more attention should be paid to the restoration and maintenance of ecological service functions, especially in areas with frequent secondary disasters to maximize the benefits of post-disaster reconstruction projects.

CRediT authorship contribution statement

Yanan Duan: Conceptualization, Methodology, Software, Writing - original draft, Writing - review & editing. **Baofeng Di:** Conceptualization, Methodology, Supervision, Funding acquisition, Writing - original draft. **Susan L. Ustin:** Conceptualization, Methodology, Writing - original draft, Writing - review & editing. **Chong Xu:** Resources, Writing - original draft. **Qiang Xie:** Resources, Validation. **Shaolin Wu:** Visualization, Data curation. **Jierui Li:** Software, Data curation. **Ruixing Zhang:** Software.

Declaration of Competing Interest

The authors declare that they have no known competing financial interests or personal relationships that could have appeared to influence the work reported in this paper.

Acknowledgments

The study received support by National Natural Science Foundation of China (Grant No. 41977245), and the Sichuan International S&T Cooperation Programme of China (Grant No. 2020YFH0060).

References

Baniya, B., Tang, Q., Pokhrel, Y., Xu, X., 2019. Vegetation dynamics and ecosystem service values changes at national and provincial scales in Nepal from 2000 to 2017. Environ. Dev. 32, 100464. https://doi.org/10.1016/j.envdev.2019.100464.

Bao, W., 2008. Ecological degradation and restoration and reconstruction countermeasures for severe calamity regions in Wenchuan earthquake in Sichuan. Bull. Chin. Acad. Sci. 324–329.
Bao, W., Pang, X., 2008. Ecological Degradation in the Wenchuan Earthquake seriously affected region in Sichuan, China. Chin. J. Appl. Environ. Biol. 14, 441–444. https://doi.org/10.3724/SP.J.1145.2008.00441.
Barral, M.P., Oscar, M.N., 2012. Land-use planning based on ecosystem service assessment: a case study in the Southeast Pampas of Argentina. Agric. Ecosyst. Environ. 154, 34–43.
Campbell, E., Marks, R., Conn, C., 2020. Spatial modeling of the biophysical and economic values of ecosystem services in Maryland, USA. Ecosyst. Serv. 43, 101093. https://doi.org/10.1016/j.ecoser.2020.101093.
Carreño, L., Frank, F.C., Viglizzo, E.F., 2012. Tradeoffs between economic and ecosystem services in Argentina during 50 years of land-use change. Agric. Ecosyst. Environ. 154, 68–77.
Chen, G., 2008. Discussion on Reconstruction of Area Hited by Wenchuan Earthquake. 26, 518-523.10.16089/j.cnki.1008-2786.2008.05.019.
Chen, F., Li, H., Zhang, A., 2019. Ecological risk assessment based on terrestrial ecosystem services in China. Acta Geogr. Sinica 74, 432–445.
Chen, M., Tang, C., Xiong, J., Shi, Q.Y., Li, N., Gong, L.F., Wang, X.D., Tie, Y., 2020. The long-term evolution of landslide activity near the epicentral area of the 2008 Wenchuan earthquake in China. Geomorphology 367, 107317. https://doi.org/10.1016/j.geomorph.2020.107317.
Chen, L., Wu, F., Yang, W., Zhang, J., 2012. A comparison on ecosystem services before/after "5.12" Wenchuan earthquake. Acta Ecol. Sinica 32 (5), 271–273.
Chiang, L.-C., Lin, Y.-P., Huang, T., Schmeller, D.S., Verburg, P.H., Liu, Y.-L., Ding, T.-S., 2014. Simulation of ecosystem service responses to multiple disturbances from an earthquake and several typhoons. Landscape Urban Plan. 122, 41–55.
Cui, P., Chen, X.-Q., Zhu, Y.-Y., Su, F.-H., Wei, F.-Q., Han, Y.-S., Liu, H.-J., Zhuang, J.-Q., 2011. The Wenchuan Earthquake (May 12, 2008), Sichuan Province, China, and resulting geohazards. Nat. Hazards 56 (1), 19–36. https://doi.org/10.1007/s11069-009-9392-1.
Cui, P., Lin, Y.-M., Chen, C., 2012. Destruction of vegetation due to geo-hazards and its environmental impacts in the Wenchuan earthquake areas. Ecol. Eng. 44, 61–69.
Di, B., Zeng, H., Zhang, M., Ustin, S.L., Tang, Y.a., Wang, Z., Chen, N., Zhang, B., 2010. Quantifying the spatial distribution of soil mass wasting processes after the 2008 earthquake in Wenchuan, China: a case study of the Longmenshan area. Remote Sens. Environ. 114 (4), 761–771.
Di, B.-F., Zhang, K.-S., Tang, Y.a., Zhang, M.-H., Ustin, S.L., 2013. The Development of a geographic information system(GIS) database for Jiuzhaigou national nature reserve and its application. J. Mt. Sci.-Engl. 10 (3), 398–409.
Ding, M., Tang, C., Huang, T., Gao, Z., Xu, C., 2020. Dynamic vulnerability analysis of mountain settlements exposed to geological hazards: a case study of the upper Min River, China. Adv. Civ. Eng. 2020, 1–13. https://doi.org/10.1155/2020/8887487.
Enming, R., Yi, X., Zhiyun, O., Hua, Z., 2016. Changes in ecosystem service of soil conservation between 2000 and 2010 and Its driving factors in Southwestern China. Chin. Geogr. Sci. 26 (2), 165–173.
Gan, B., Yang, X., Zhang, W., Zhou, J., 2019. Temporal and spatial evolution of vegetation coverage in the Mianyuan River Basin influenced by strong earthquake disturbance. Sci. Rep.-Uk 9, 16762. https://doi.org/10.1038/s41598-019-53264-5.
Gao, Q., Zhu, W., Schwartz, M.W., Ganjurjav, H., Wan, Y., Qin, X., Ma, X., Williamson, M.A., Li, Y., 2016. Climatic change controls productivity variation in global grasslands. Sci. Rep.-Uk 6, 26958. https://doi.org/10.1038/srep26958.
Komugabe-Dixson, A.F., de Ville, N.S.E., Trundle, A., McEvoy, D., 2019. Environmental change, urbanisation, and socio-ecological resilience in the Pacific: community narratives from Port Vila, Vanuatu. Ecosyst. Serv. 39, 100973. https://doi.org/10.1016/j.ecoser.2019.100973.
Lee, J., Kim, H., Song, C., Kim, G.S., Lee, W.-K., Son, Y., 2020. Determining economically viable forest management option with consideration of ecosystem services in Korea: a strategy after successful national forestation. Ecosyst. Serv. 41, 101053. https://doi.org/10.1016/j.ecoser.2019.101053.
Lin, W.-T., Lin, C.-Y., Chou, W.-C., 2006. Assessment of vegetation recovery and soil erosion at landslides caused by a catastrophic earthquake: a case study in Central Taiwan. Ecol. Eng. 28 (1), 79–89.
Liu, J., Zou, C., Gao, J., Ma, S., Wang, W., Wu, K., Liu, Y., 2015. Location determination of ecologically vulnerable regions in China. Biodivers. Sci. 23, 725–732. https://doi.org/10.17520/biods.2015147.
Liu, L., Wang, Z., Wang, Y., Zhang, Y., Shen, J., Qin, D., Li, S., 2019. Trade-off analyses of multiple mountain ecosystem services along elevation, vegetation cover and precipitation gradients: a case study in the Taihang Mountains. Ecol. Ind. 103, 94–104.
Lu, F., Hu, H., Sun, W., Zhu, J., Liu, G., Zhou, W., Zhang, Q., Shi, P., Liu, X., Wu, X., 2018. Effects of national ecological restoration projects on carbon sequestration in China from 2001 to 2010. Proc. Natl. Acad. U. S. A. 115 (16), 4039–4044.
Mace, G., Masundire, H., Baillie, J., 2005. Ecosystems and human well-being: Current state and trends: findings of the Condition and Trends Working Group. Millennium Ecosyst. Assess.. 2–20.
MEA, M., 2005. Ecosystems and Human Well-Being: Desertification Synthesis. Millennium Ecosystem Assessment.
Ministry of Environmental Protection, 2015. Technical Guidelines for the Demarcation of Ecological Protection Red Lines. Ministry of Environmental Protection of the People's Republic of China, Beijing.
Nguyen, K., Liou, Y., 2019. Global mapping of eco-environmental vulnerability from human and nature disturbances. Sci. Total Environ. 664, 995–1004.
Ouyang, Z., Xu, W., Wang, X., Wang, W., Dong, R., Zheng, H., Li, D., Li, Z., Zhang, H., Zhuang, C., 2008. Impact assessment of Wenchuan Earthquake on ecosystems. Acta Ecol. Sin. 28, 5801–5809.
Peng, J., Liu, Y., Wu, J., Lv, H., Hu, X., 2015. Linking ecosystem services and landscape patterns to assess urban ecosystem health: a case study in Shenzhen City, China. Landscape Urban Plan. 143, 56–68.
Peng, W., Kuang, T., Tao, S., 2019. Quantifying influences of natural factors on vegetation NDVI changes based on geographical detector in Sichuan, western China. J Clean Prod. 233, 353–367.
Pham, H.V., Sperotto, A., Torresan, S., Acuña, V., Jorda-Capdevila, D., Rianna, G., Marcomini, A., Critto, A., 2019. Coupling scenarios of climate and land-use change with assessments of potential ecosystem services at the river basin scale. Ecosyst. Serv. 40, 101045. https://doi.org/10.1016/j.ecoser.2019.101045.
Sannigrahi, S., Zhang, Q., Joshi, P.K., Sutton, P.C., Keesstra, S., Roy, P.S., Pilla, F., Basu, B., Wang, Y., Jha, S., Paul, S.K., Sen, S., 2020. Examining effects of climate change and land use dynamic on biophysical and economic values of ecosystem services of a natural reserve region. J Clean Prod. 257, 120424. https://doi.org/10.1016/j.jclepro.2020.120424.
Shafique, M., 2020. Spatial and temporal evolution of co-seismic landslides after the 2005 Kashmir earthquake. Geomorphology 362, 107228. https://doi.org/10.1016/j.geomorph.2020.107228.
Talukdar, S., Singha, P., Mahato, Shahfahad, S., Praveen, B., Rahman, A., 2020. Dynamics of ecosystem services (ESs) in response to land use land cover (LU/LC) changes in the lower Gangetic plain of India. Ecol. Ind. 112, 106121. https://doi.org/10.1016/j.ecolind.2020.106121.
Wang, H., Liu, G., Li, Z., Zhang, L., Wang, Z., 2020. Processes and driving forces for changing vegetation ecosystem services: Insights from the Shaanxi Province of China. Ecol. Ind. 112, 106105. https://doi.org/10.1016/j.ecolind.2020.106105.
Wang, J., Xu, C., 2017. Geodetector: principle and prospective. Acta Geogr. Sinica 72, 116–134.
Wang, Y.K., Fu, B., Xu, P., 2012. Evaluation the impact of earthquake on ecosystem services. Procedia Environ. Sci. 13, 954–966.
Wang, Z., Zhang, Y., Yang, Y., Zhou, W., Gang, C., Zhang, Y., Li, J., An, R., Wang, K., Odeh, I., Qi, J., 2016. Quantitative assess the driving forces on the grassland degradation in the Qinghai-Tibet Plateau, in China. Ecol. Inform. 33, 32–44.
Wu, N., Lu, T., Luo, P., Zhu, D., 2008. A review of the impacts of earthquake on mountain ecosystems: taking 5.12 Wenchuan Earthquake as an example. Acta Ecol. Sinica 28, 5810–5819.
Xu, C., Xu, X., Shen, L., Yao, Q., Tan, X., Kang, W., Ma, S., Wu, X., Cai, J., Gao, M., Li, K., 2016. Optimized volume models of earthquake-triggered landslides. Sci. Rep.-Uk 6, 29797. https://doi.org/10.1038/srep29797.
Xu, C., Xu, X., Yao, X., Dai, F., 2014. Three (nearly) complete inventories of landslides triggered by the May 12, 2008 Wenchuan Mw 7.9 earthquake of China and their spatial distribution statistical analysis. Landslides 11 (3), 441–461.
Yang, W., Qi, W., Zhou, J., 2018. Decreased post-seismic landslides linked to vegetation recovery after the 2008 Wenchuan earthquake. Ecol. Ind. 89, 438–444.
Yunus, A.P., Fan, X., Tang, X., Jie, D., Xu, Q., Huang, R., 2020. Decadal vegetation succession from MODIS reveals the spatio-temporal evolution of post-seismic landsliding after the 2008 Wenchuan earthquake. Remote Sens. Environ. 236, 111476. https://doi.org/10.1016/j.rse.2019.111476.
Zhang, J., Hull, V., Xu, W., Liu, J., Ouyang, Z., Huang, J., Wang, X., Li, R., 2011. Impact of the 2008 Wenchuan earthquake on biodiversity and giant panda habitat in Wolong Nature Reserve, China. Ecol Res. 26 (3), 523–531.
Zhang, J., Hull, V., Huang, J., Yang, W., Zhou, S., Xu, W., Huang, Y., Ouyang, Z., Zhang, H., Liu, J., 2014. Natural recovery and restoration in giant panda habitat after the Wenchuan earthquake. Forest Ecol. Manag. 319, 1–9.
Zhang, X., Wang, M., Liu, K., Xie, J., Xu, H., 2018a. Using NDVI time series to diagnose vegetation recovery after major earthquake based on dynamic time warping and lower bound distance. Ecol. Ind. 94, 52–61.
Zhang, R., Liang, T., Guo, J., Xie, H., Feng, Q., Aimaiti, Y., 2018b. Grassland dynamics in response to climate change and human activities in Xinjiang from 2000 to 2014. Sci. Rep.-Uk 8, 2888. https://doi.org/10.1038/s41598-018-21089-3.
Zhang, Z., Liu, Y., Wang, Y., Liu, Y., Zhang, Y., Zhang, Y., 2020a. What factors affect the synergy and tradeoff between ecosystem services, and how, from a geospatial perspective? J. Clean Prod. 257, 120454. https://doi.org/10.1016/j.jclepro.2020.120454.
Zhang, Z., Xia, F., Yang, D., Huo, J., Wang, G., Chen, H., 2020b. Spatiotemporal characteristics in ecosystem service value and its interaction with human activities in Xinjiang, China. Ecol Indic. 110, 105826. https://doi.org/10.1016/j.ecolind.2019.105826.
Zhen, L., Hu, Y., Wei, Y., Qi, L., Han, Y., 2019. Trend of ecological degradation and restoration technology requirement in typical ecological vulnerable regions. Resour. Sci. 41, 63–74. https://doi.org/10.18402/resci.2019.01.07.
Zhao, Y., Deng, Q., Lin, Q., Cai, C., 2017. Quantitative analysis of the impacts of terrestrial environmental factors on precipitation variation over the Beibu Gulf Economic Zone in Coastal Southwest China. Sci. Rep.-Uk 7, 44412. https://doi.org/10.1038/srep44412.
Zhou, J., Zhao, Y., Huang, P., Zhao, X., Feng, W., Li, Q., Xue, D., Dou, J., Shi, W., Wei, W., Zhu, G., Li, C., 2020. Impacts of ecological restoration projects on the ecosystem carbon storage of inland river basin in arid area, China. Ecol. Ind. 118, 106803. https://doi.org/10.1016/j.ecolind.2020.106803.